Surface & Coatings Technology 478 (2024) 130467

Contents lists available at ScienceDirect

Surface & Coatings Technology

journal homepage: www.elsevier.com/locate/surfcoat

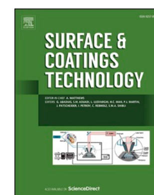

# Effect of the TiSiN interlayer properties on the adhesion and mechanical properties of multilayered TiSiCN thin films

Wolfgang Tillmann [a], Julia Urbanczyk [a,*], Alexander Thewes [b], Günter Bräuer [b], Nelson Filipe Lopes Dias [a]

[a] *Institute of Materials Engineering, TU Dortmund University, Leonhard-Euler-Straße 2, 44227 Dortmund, Germany*
[b] *Institute for Surface Technology, TU Braunschweig, Field Office Dortmund, Eberhardstr. 12, p-4415 Dortmund, Germany*

ARTICLE INFO

*Keywords:*
TiSiCN
Magnetron sputtering
Bias voltage
Adhesion
Multilayer design
Residual stress

ABSTRACT

The interlayer design is crucial in optimizing the adhesion of TiSiCN thin films on tool steel. Thus, Ti/TiN/TiSiN interlayer systems were deposited varying the TiSiN interlayer bias voltages (−100 V, −150 V, −200 V) in a magnetron sputtering process to investigate the influence on the mechanical properties and adhesion of the TiSiCN top layer with different thicknesses.

A higher bias voltage densifies the TiSiN interlayer structure, thereby increasing its residual stresses (0.11 GPa to 1.46 GPa) and hardness (28.1 GPa to 34.9 GPa). This occurs without affecting the columnar-like microstructure of the TiSiCN top layer and its hardness (25.9 GPa to 29.1 GPa for $t = 1.0$ μm, 22.6 GPa to 24.8 GPa for $t = 2.3$ μm). Adhesion classification by Rockwell C indentation of TiSiN declined from HF2 to HF4 due to increased residual stresses, impacting TiSiCN top layer adhesion with a similar deterioration. Scratch tests revealed reduced critical loads $L_{c2}$ and $L_{c3}$ for the TiSiN interlayer system and also for TiSiCN top layers. The highest critical loads were observed for TiSiCN (1.0 μm) and TiSiCN (2.3 μm) with TiSiN interlayer deposited at a bias voltage of −100 V, measuring (64.4 ± 4.5) N and (73.4 ± 8.3) N for $L_{c2}$, and (57.4 ± 5.3) N and (71.6 ± 4.5) N for $L_{c3}$, respectively. Increasing bias voltage decreases $L_{c2}$ and $L_{c3}$ to (23.2 ± 4.5) N and (50.20 ± 2.2) N for TiSiCN (1.0 μm), and (21.4 ± 4.5) N and (58.0 ± 3.6) N for TiSiCN (2.3 μm).

Achieving high adhesion strength of TiSiCN multilayered system requires minimizing the residual stress differences between the layers. Therefore, when designing a complex multilayer structure for TiSiCN thin films, careful consideration of the stress state among the layers is crucial, which is achieved by adjusting the bias voltage.

## 1. Introduction

The ternary TiSiN and TiCN thin film systems are a further development of the binary TiN. TiCN reveals higher hardness and wear resistance than TiN [1,2] while exhibiting lower internal stresses and, consequently, improved adhesion compared to TiC [3]. TiSiN also presents enhanced hardness [4,5] and abrasion resistance [6] in relation to TiN. To further expand and combine the mechanical properties of TiSiN and TiCN, the quaternary TiSiCN thin film systems were developed. TiSiCN consists of a nanocomposite structure with nanocrystallites of TiN and TiC, which are embedded by an amorphous matrix of Si- and C-based phases [7–9]. It was demonstrated that TiSiCN thin films have improved hardness exceeding 40 GPa and oxidation resistance than TiCN and TiSiN [10–12]. Moreover, the presence of self-lubricating amorphous Si- and C-based phases contributes to reduced friction and wear [7,12,13]. However, hard TiSiCN layers are characterized by high compressive residual stresses, which results in poor adhesion on metallic substrates [10,14,15]. To maintain the integrity and adhesion of hard thin films, it is crucial to reduce substantial disparities in elastic modulus and hardness between the thin film and substrate [16].

To improve the adhesion strength of TiSiCN, it is common to deposit a multilayered thin film structure with a functional TiSiCN top layer. It has been demonstrated that chemically graded interlayers contribute to improved adhesion strength of the top layer. In this regard, previous studies synthesized bi- or multilayer thin films with chemical gradients [10,14,15,17]. Chang et al. deposited TiSiCN thin films on WC-Co substrate without and with a Ti/TiN/TiSiN interlayer system using a dual cathodic arc plasma evaporation system and obtained improved

* Corresponding author.
*E-mail address:* julia.urbanczyk@tu-dortmund.de (J. Urbanczyk).

https://doi.org/10.1016/j.surfcoat.2024.130467
Received 18 July 2023; Received in revised form 19 January 2024; Accepted 23 January 2024
Available online 26 January 2024
0257-8972/© 2024 The Author(s). Published by Elsevier B.V. This is an open access article under the CC BY-NC-ND license (http://creativecommons.org/licenses/by-nc-nd/4.0/).

adhesion compared to a TiSiCN thin film without interlayer [15]. Abdollah-Zadeh et al. deposited TiSiCN with a graded Ti/TiN/TiCN interlayer on plasma nitrided H13 hot-working tool steel by plasma-enhanced chemical vapor deposition and noted an improved toughness, adhesion, and wear resistance [17].

Besides the application of multilayers with chemical gradients, the consideration of the stress state within the thin film system is also decisive for the adhesion behavior. In a previous study, the authors varied the bias voltage for the deposition of a chemically graded $Ti_xC_y$ interlayer with an amorphous carbon top layer and demonstrated that an interlayer with low stresses improved the adhesion of the entire thin film structure [18]. Li et al. successfully enhanced the adhesion strength of the complete thin film system by employing a stress-graded TiN interlayer during the arc ion plating deposition of TiSiCN, although specific details regarding the stress adjustment were not provided [19].

In addition to the interlayer design, the applied bias voltage is a critical deposition parameter, that allows the tailoring of mechanical properties of thin films. Higher negative bias voltages induce intensified ion bombardment of the deposited layer, causing a denser and more compact microstructure with improved hardness, but concurrently higher compressive stresses [18,20]. Previous studies already demonstrated that an interlayer design with a chemical gradient, such as Ti/TiN/TiSiN is beneficial to improve the adhesion strength of TiSiCN on the substrate [15]. However, the effect of the bias voltage on the interlayer properties and their interaction with the mechanical properties and adhesion behavior of the TiSiCN top layer has not been addressed so far. Nevertheless, it can be used to control the stress state and hardness of the interlayer and consequently improve the adhesion behavior. It is expected that adjusting the TiSiN interlayer properties will directly influence the adhesion strength of the TiSiCN on the substrate.

Previous studies of TiSiN thin films demonstrated that high bias voltages lead to enhanced hardness of up to 46 GPa accompanied by increasing residual stresses [21–23]. Additionally, the adhesion behavior of TiSiN improved with increasing bias voltage up to −150 V. A further rise of the bias voltage reduced adhesion strength due to high level of compressive stresses [23]. Also, enhanced scratch adhesion strength of TiSiN was found to correlate with a dense thin film structure induced by higher bias voltage and therefore higher hardness and elastic modulus values but high residual stress which promote a brittle character [24]. These studies focused on the influence of the bias voltage on the properties of TiSiN thin films, but not on TiSiN interlayers and their interaction with the TiSiCN top layer.

Therefore, adjusting the bias voltage during the TiSiN interlayer growth is a promising approach to control and adjust the interlayer properties and, consequently, enhancing the adhesion strength of the TiSiCN top layer. In a magnetron sputtering process, the TiSiCN thin films of different thicknesses were deposited with a chemical-graded interlayer structure of Ti/TiN/TiSiN. The bias voltage of the TiSiN layer was deposited under different bias voltages (BV) of $U_b = -100$, −150, and − 200 V. Ti/TiN/TiSiN interlayer structures and Ti/TiN/TiSiN/TiSiCN multilayers were analyzed to evaluate the influence of the bias voltage of the TiSiN layer on the mechanical properties and adhesion of the TiSiCN top layer.

## 2. Experimental details

### 2.1. Deposition setup

The TiSiCN thin films were deposited using an industrial magnetron sputtering device CC800/9 Custom (CemeCon AG, Germany) which is schematically shown in Fig. 1. One Ti target and three $Ti_{80}Si_{20}$ targets (Plansee Composite Material GmbH, Germany) were mounted on the magnetron cathodes. The rectangular-shaped targets had an area of 88 × 500 mm$^2$. High-speed steel (AISI M2) with a diameter of 30 mm, a thickness of 5 mm, and 60 HRC and n-type Si(100) wafers with a

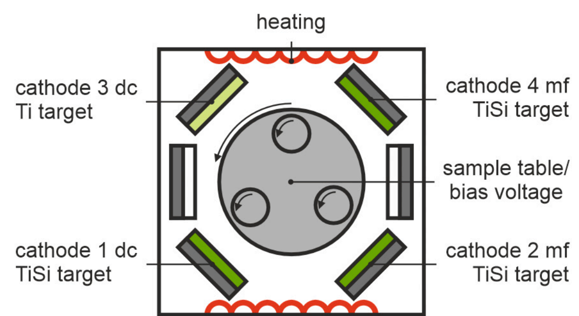


**Fig. 1.** Magnetron sputtering set up for the desposition of TiSiN and TiSiCN mulitlayer systems with TiSiN grown at a bias voltage $U_b$ of −100, −150, and −200 V

dimension of 10 × 50 mm$^2$ served as substrate material and were ultrasonically cleaned in ethanol for 15 min. The deposition chamber was evacuated to a base pressure below 5 mPa. The deposition chamber has size of 850 × 850 × 1.000 mm$^3$, the deposition room exhibits a diameter of 400 mm and a height of 400 mm. The distance between target and substrate was approximately 170 mm. Before deposition, the substrates were etched by $Ar^+$ ions at a pulsed BV of $U_b = -650$ V with a mid-frequency of $f = 350$ kHz for $t = 30$ min. In the first deposition step, a metallic 200 nm Ti layer was sputtered from the Ti target at a cathode power of $P_c = 4$ kW and a direct current bias voltage (dc-BV) of $U_b = -100$ V in an Ar-regulated pressure of $p = 350$ mPa. The second TiN layer with 300 nm thickness was applied by adding an $N_2$ gas flow of $q_{N2} = 70$ sccm in an $N_2$-regulated pressure of $p = 350$ mPa. The next 500 nm TiSiN interlayer was deposited from one of the three $Ti_{80}Si_{20}$ targets with a variation of the dc-BV $U_b$ of −100 V, −150 V, and − 200 V at the gas flow and pressure mentioned before. Finally, TiSiCN with 1.0 μm or 2.3 μm thickness was sputtered with the addition of 10 sccm $C_2H_2$ at a mid-frequency bias voltage (mf-BV) of $U_b = -100$ V, a frequency of $f = 350$ kHz and a pulse duration of $t = 500$ ns. The cathode power of the $Ti_{80}Si_{20}$ targets was set at $P_c = 5$ kW each at an Ar-regulated pressure of $p = 350$ mPa. The applied heating power for all deposition steps was maintained at $P_h = 5$ kW, resulting in a heater temperature of approximately 610 °C. Besides the Ti/TiN/TiSiN/TiSiCN multilayers, Ti/TiN/TiSiN interlayer systems only were deposited to investigate the effect of the different BV on the interlayer properties of TiSiN. For simplification, the interlayer system Ti/TiN/TiSiN will be labeled as TiSiN, and the multilayer system with TiSiCN top layer will be presented as TiSiCN (1.0 μm) and TiSiCN (2.3 μm) according to their thickness.

### 2.2. Characterization of the thin films

The chemical composition was quantitatively determined using an electron probe microanalyzer (EPMA) equipped with four wavelength-dispersive x-ray spectroscopy (WDS). The acceleration voltage was set to 10 keV at a beam current of 20 nA. The counting times were 10 s for the peak and 5 s for the background signal. The beam diameter was 5 μm. To analyze the crystalline phases of the multilayer systems x-ray diffraction (XRD) analysis was performed. Cu-Kα1 radiation with a wavelength of $\lambda = 1.5406$ Å and a x-ray polycapillary lens of 2 mm diameter were used. The locked-couple scan range $2\theta$ was set from 30° to 50° with a scan step of $\Delta 2\theta = 0.034°$ and an exposure time of 1 s. The microstructure and surface morphology of the multilayer systems were analyzed by secondary electron imaging of scanning electron microscopy (SEM). Roughness measurements were performed with confocal microscopy TOOLinspect (confovis GmbH, Germany). The residual stresses were determined from the substrate curvature using Stoney's equation [25]. For this purpose, the curvature radius of the coated Si wafers was measured using a contour measurer MarSurf XC 20 (Mahr GmbH, Germany) with a feed rate of 0.2 mm/s and a contact force of 0.01 N to measure the radius of the deposited Si wafer due to the change

of its curvature by residual stresses in the thin film systems after deposition. The hardness and elastic modulus of the thin films were determined by nanoindentation with a Berkovich diamond tip working in continuous stiffness mode, as proposed by Oliver and Pharr [26]. A total of 49 indents in an array of 7 × 7 with a distance of 50 μm between each measurement were performed on each multilayer system. The hardness and elastic modulus were evaluated up to 10 % of the film thickness to avoid influences of the substrate. A Poisson's ratio of 0.20 for TiSiN [27,28] and 0.25 for TiSiCN [8] was considered for the calculation of the elastic modulus. The adhesion behavior of the TiSiN and TiSiCN multilayer systems on an HSS substrate was evaluated in Rockwell C indentation tests at a load of 1471.5 N (150 kgf) according to the German standard DIN 4856:2018–02 [29]. The Rockwell C indents were examined by SEM as well as energy dispersive x-ray spectroscopy (EDS) and categorized into the adhesion classes from HF1 (excellent adhesion) to HF6 (poor adhesion). Additionally, scratch tests were performed using a Revetest (CSM Instruments SA, Switzerland) equipped with a Rockwell C diamond tip with a radius curvature of 200 μm according to DIN EN ISO 20502:2016–11 [30]. The scratches were evaluated in SEM and EDS and the critical loads $L_{c2}$ and $L_{c3}$ were determined.

## 3. Results and discussion

### 3.1. Chemical composition and structure of the TiSiN and TiSiCN thin films

The TiSiN interlayers show no noticeable changes in the chemical composition regarding Ti, Si, and N with an increasing BV (see Table 1). In this regard, Ti ranges from 35.81 to 36.71 at.-%, Si from 8.75 to 9.90 at.-% and N from 49.66 to 50.99 at.-%. It is noted that the amount of Ar increases with a higher BV from (0.29 ± 0.01) at.-% ($U_b = -100$ V) to (0.52 ± 0.03) at.-% ($U_b = -150$ V) to (1.45 ± 0.03) at.-% ($U_b = -200$ V) due to an increased $Ar^+$ ion bombardment of the growing film, which also is typically observed for sputtered thin films due to Ar implantation [31–33].

**Table 1**
Chemical composition of the TiSiN interlayer and the TiSiCN top layer of 1.0 μm or 2.3 μm thickness with TiSiN grown at a bias voltage $U_b$ of −100, −150, and −200 V, obtained by EPMA.

| Multi-layer system | Bias voltage of TiSiN interlayer [-V] | Chemical composition [at.-%] | | | | | |
|---|---|---|---|---|---|---|---|
| | | Ti | Si | N | Ar | O | C |
| TiSiN | 100 | 36.27 ± 0.64 | 9.90 ± 0.41 | 49.66 ± 0.45 | 0.29 ± 0.01 | 3.88 ± 0.06 | – |
| | 150 | 36.71 ± 0.88 | 8.75 ± 0.33 | 50.82 ± 0.79 | 0.52 ± 0.03 | 3.19 ± 0.23 | – |
| | 200 | 35.81 ± 0.58 | 9.46 ± 0.19 | 50.99 ± 0.65 | 1.45 ± 0.03 | 2.56 ± 0.13 | – |
| TiSiCN (1.0 μm) | 100 | 36.69 ± 0.86 | 8.19 ± 0.09 | 42.20 ± 0.38 | 0.28 ± 0.01 | 2.30 ± 0.18 | 10.34 ± 0.41 |
| | 150 | 36.26 ± 0.28 | 8.21 ± 0.12 | 42.58 ± 0.65 | 0.29 ± 0.01 | 2.35 ± 0.16 | 10.30 ± 0.27 |
| | 200 | 35.82 ± 0.59 | 8.00 ± 0.37 | 43.23 ± 0.35 | 0.29 ± 0,03 | 2.35 ± 0.23 | 10.47 ± 0.25 |
| TiSiCN (2.3 μm) | 100 | 35.73 ± 0.46 | 8.37 ± 0.20 | 43.25 ± 0.28 | 0.23 ± 0.01 | 2.56 ± 0.23 | 9.93 ± 0.12 |
| | 150 | 34.61 ± 0.31 | 8.37 ± 0.24 | 43.27 ± 0.47 | 0.24 ± 0.01 | 2.61 ± 0.50 | 11.25 ± 0.29 |
| | 200 | 36.49 ± 0.42 | 8.29 ± 0.09 | 42.11 ± 0.67 | 0.25 ± 0.01 | 2.30 ± 0.15 | 10.55 ± 0.33 |

The TiSiN interlayers as well as both TiSiCN top layers contain comparable Ti and Si contents. In this regard, both TiSiCN thin films have an amount of Ti around 34.61–36.49 at.-% and an amount of Si around 8.00–8.37 at.-%. The addition of C to TiSiN in the top layers leads to a decrease in N due to the higher chemical activity of C compared to N. As a consequence, C prefers to bond with Ti and Si [19]. The C content for TiSiCN (1.0 μm) and TiSiCN (2.3 μm) top layer reaches 9.93–11.25 at.-%, while the N content is around 42.11–43.27 at.-%. The Ar content for TiSiCN (1.0 μm) is around 0.28–0.29 at.-% and for TiSiCN (2.3 μm) around 0.23–0.25 at.-%. The Ar incorporation within the TiSiCN layers is similar to TiSiN deposited at a BV of $U_b = -100$ V.

Fig. 2 shows XRD patterns of the multilayered TiSiN interlayers as well as the TiSiCN top layers of 1.0 μm and 2.3 μm thickness. For all thin films, the diffractions show Bragg reflections of the substrate material, which are assigned to α-Fe at 44.6° and the $Me_6C$ carbide at 42.5° and 40.0°. In addition, all thin film systems contain the cubic β-Ti phase with a preferred orientation along the (111) plane, which stems from the Ti interlayer. For the TiSiN interlayer grown at a BV of $U_b = -100$ V, the diffraction pattern presents a broad diffraction angle from 36.0° to 37.6° with an asymmetrical diffraction angle towards lower angles. The peak intensity is around 36.6° and can be identified as TiN (111) of the TiN interlayer. In TiAlN thin films, a higher BV benefits the incorporation of Al into the TiN lattice. This phenomenon is accompanied by a reduction in the intensity of the TiN (111) peak, which can be attributed to the enhanced ion bombardment [34]. However, Arab Pour Yazdi et al. reported this effect solely in TiSiN thin films with a low Si content of up to 3 at.-% with a crystalline structure [35]. The TiSiN thin films examined in this study contain up to 10 at.-% of Si and, as described by Patscheider et al., should exhibit TiN crystallites embedded within an amorphous Si-based matrix [36]. Consequently, the presence of the right shoulder around 37.0° indicates the superposition of the enclosed crystalline TiN (111) phase of the TiSiN interlayer, characterized by a peak shift towards lower diffraction angles attributed to increased residual stresses resulting from higher BV. Hence, the Bragg diffraction observed for TiSiN deposited at a BV of $U_b = -100$ V is a superposition of the TiN phase of the TiN interlayer and the TiN phase of the TiSiN interlayer. At higher BV values, the peak for the (111) planes of TiSiN shifts towards lower angles, whereas the diffraction angle at 42.5° shows an increased intensity and width. This is attributed to the intensified ion bombardment during the film growth, resulting in shifting preferential growth of TiN along the energetic favorable (200) orientation [37,38].

For the TiSiCN top layers, the diffractograms indicate the presence of the TiC phase with Bragg reflections at 35.7°, which is assigned to TiC (111). Furthermore, a shoulder formation of the Bragg angle at 37.0° is observed for TiSiCN with a TiSiN interlayer deposited at $U_b = -100$ V, which can be assigned to the TiSiN interlayer as previously noted. Moreover, the diffraction angle of TiSiN (200) reveals a higher intensity. In this regard, TiSiCN thin films with a thickness of 2.3 μm show a higher intensity compared to the thin films with a thickness of 1.0 μm, indicating a higher amount of the TiSiN phases and/or a higher crystallinity. In previous studies, the crystalline TiC and TiN phases were commonly identified for TiSiCN nanocomposites [7,9,19]. There were no signals detected related to crystalline Si-base phases, such as SiN or SiC.

The SEM micrographs of the multilayer structures are shown in Fig. 3. The Ti and TiN interlayer show a typical columnar-like structure. The TiSiN thin film deposited at a BV of $U_b = -100$ V also exhibits a columnar growth, which changes progressively to a dense structure with increasing BV due to the intensified ion bombardment. It is noted that the TiSiN interlayer does not affect the microstructure of the TiSiCN top layer. In this regard, the TiSiCN thin films reveal a columnar-like structure as well. With higher thickness, the columnar-like structure of the TiSiCN top layer coarsens. Similar structure formations for TiSiCN with relatively low Si and C contents were also observed in previous studies [39,40].

Fig. 4 shows the SEM micrographs of the surface morphology of the

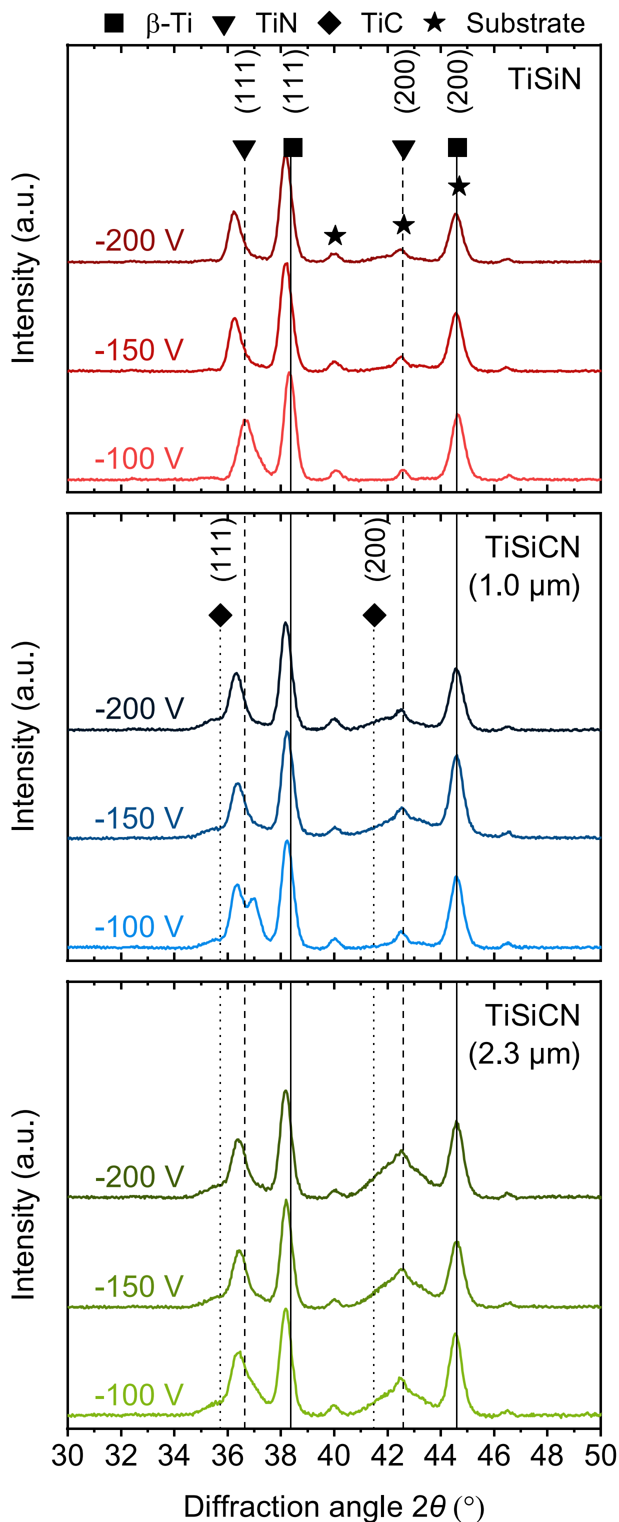


**Fig. 2.** XRD patterns of the TiSiN interlayer and the TiSiCN top layer of 1.0 μm and 2.3 μm thickness with TiSiN grown at bias voltages $U_b$ of −100, −150, and − 200 V.

TiSiN interlayers and the TiSiCN top layers of different thicknesses. The surface of the TiSiN interlayer changes from a cauliflower-like structure at $U_b = -100$ V to a surface with crate-like structures at $U_b = -200$ V. The measured roughness of the TiSiN surfaces tends to roughen with higher BV (see Fig. 5). With increasing BV, the *Ra* values of the TiSiN interlayers rise from (8.9 ± 0.5) nm for $U_b = -100$ V to (12.1 ± 0.3) nm for $U_b = -200$ V. *Rz* shows a similar trend as *Ra* and increases from (113.9 ± 20.1) nm to (103.8 ± 2.2) nm to (123.0 ± 5.9) nm. In a previous study, Yang et al. noted a decrease in roughness for TiSiN thin films with increasing BV up to $U_b = -100$ V as a result of densification due to the intensified ion bombardment. This is in good agreement with the present results. With higher BV up to $U_b = -250$ V, roughness increases because of the rising mobility of Ti [41]. While the roughness of TiAlN increases in the range of 0 V to −150 V according to more induced damages at higher BV values [34]. A similar trend can be observed here.

The roughness of the top layer of the TiSiCN (1.0 μm) system is not affected by the TiSiN interlayer roughness due to higher ion bombardment. *Rz* ranges from 127.6 nm to 132.6 nm and *Ra* from 12.3 nm to 13.5 nm. For TiSiCN (2.3 μm) *Rz* reaches values from 204.1 nm to 230.8 nm and *Ra* from 20.4 nm to 24.1 nm. An increasing roughness with a larger thickness is typically observed for PVD thin films. With the rise of TiSiCN top layer thickness from 1.0 μm to 2.3 μm, the roughness increases due to more preferred crystal orientation and shadowing effects accompanied by coarsening with increasing film thickness [42]. In general, the variation in surface morphology of the TiSiN interlayer due to higher bias voltages does not influence the growth and surface morphology of the TiSiCN top layers which shows comparable surface structures and roughness values.

### 3.2. Mechanical properties of the TiSiN and TiSiCN thin films

The residual stresses of the Ti/TiN/TiSiN and Ti/TiN/TiSiN/TiSiCN thin film systems were determined from the Si substrate curvature and are presented in Fig. 6. For the Ti/TiN/TiSiN interlayer systems, the residual stress increases from (0.11 ± 0.04) GPa at $U_b = -100$ V to (1.46 ± 0.12) GPa at $U_b = -200$ V (see Fig. 6). An increased ion bombardment induces higher compressive residual stress into the TiSiN interlayer due to more defect generation [22,24]. Moreover, the rise in Ar implantation contributes to additional lattice distortion leading to elevated residual stresses [43]. This can be also observed in the shoulder formation of the TiN (111) diffraction angle which shifts to lower 2θ as a result of higher stress within the TiSiN thin films. The influence of the residual stress of the TiSiN interlayer is present for both TiSiCN top layers, which overall demonstrate higher residual stress with highly stressed TiSiN interlayers. The pronounced increase in residual stress for TiSiCN (1.0 μm) with TiSiN deposited at $U_b = -200$ V may be attributed to pronounced dislocation and lattice mismatches between the TiSiN interlayer and the TiSiCN top layer [44].

For the TiSiCN (1.0 μm) multilayer system, the residual stresses rise from (0.26 ± 0.00) GPa to (0.83 ± 0.19) GPa, and for TiSiCN (2.3 μm) from (0.15 ± 0.11) GPa to (0.56 ± 0.10) GPa. It is noted that an increase in the thickness of the TiSiCN top layer contributes to a reduction in residual stresses. This can be attributed to the coarsening of the thin film structure, which is more pronounced in thicker films [45]. For bilayered Ti/TiN systems, Huang et al. reported a coarser TiN microstructure aligns easier on the Ti interlayer which acts as a growth template, resulting in lower residual stresses [46]. Generally, the coarser and softer structure of the TiSiCN top layer absorbs the energy of the harder TiSiN layer [47]. As a result, the higher thickness of the TiSiCN layer leads to a mitigation of residual stresses within the multilayer system.

The hardness and elastic modulus of the TiSiN and TiSiCN thin film systems were determined in nanoindentation tests and are shown in Fig. 7. The TiSiN interlayer shows an increase in hardness from (28.1 ± 2.7) GPa to (34.9 ± 4.5) GPa with higher BV due to the densification caused by intensified ion bombardment. This is in good agreement with the results of previous studies [21,41,48]. Furthermore, the elevated residual stresses of TiSiN also contribute to the higher hardness values [49]. Consequently, the $H/E$ and $H^3/E^2$ ratios also show an increase, indicating an extended range of elastic strain to failure and enhanced resistance against plastic deformation in the TiSiN thin film [50]. The TiSiCN top layer shows similar hardness and elastic modulus values as reported in other works [9,51,52]. The hardness for 1.0 μm TiSiCN is

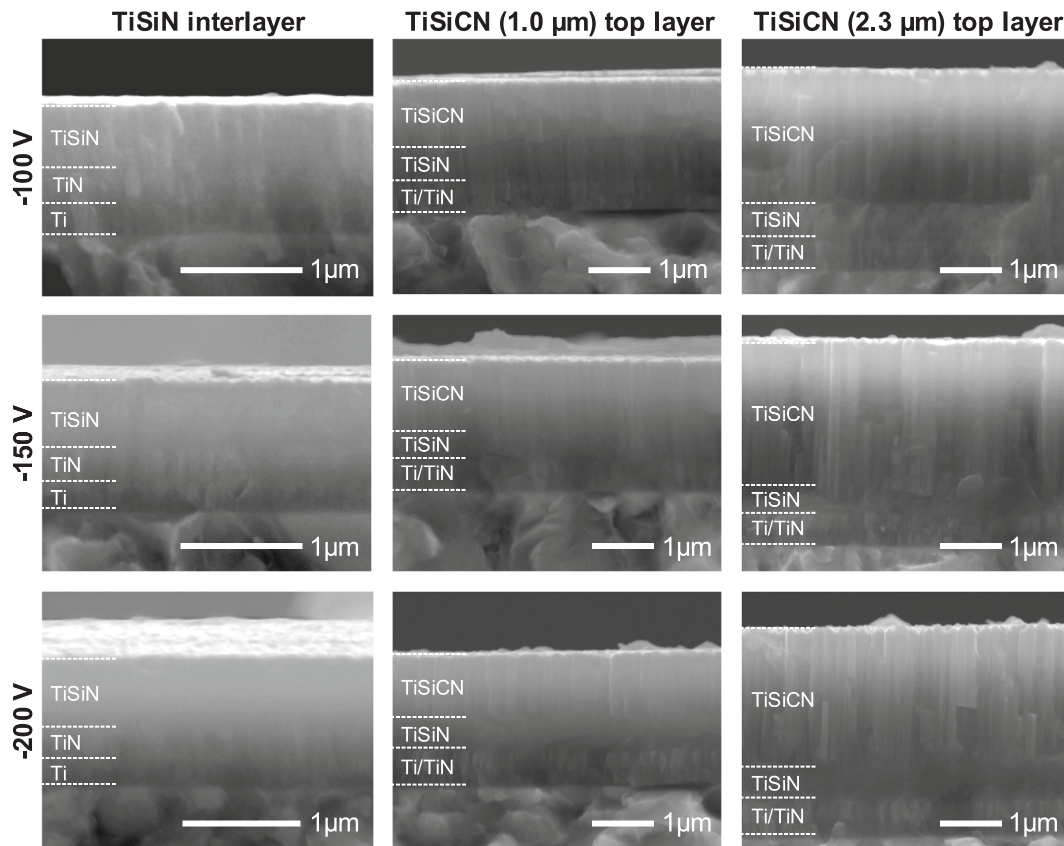


**Fig. 3.** SEM micrographs of the microstructure of the TiSiN interlayer and the TiSiCN top layer of 1.0 μm and 2.3 μm thickness with TiSiN grown at bias voltages $U_b$ of −100, −150, and − 200 V.

(26.6 ± 1.8) GPa ($U_b$ = −100 V), (25.9 ± 2.0) GPa ($U_b$ = −150 V), and (29.1 ± 1.6) GPa ($U_b$ = −200 V). Only the hardness of TiSiCN (1.0 μm) significantly increases when combined with TiSiN deposited at $U_b$ = −200 V due to a more pronounced rise in residual stress within this interlayer system. Overall, the hardness of TiSiCN (1.0 μm) top layer exhibits a higher hardness compared to TiSiCN (2.3 μm), which exhibits values of (23.4 ± 1.8) GPa ($U_b$ = −100 V), (24.8 ± 1.2) GPa ($U_b$ = −150 V), and (22.6 ± 1.6) GPa ($U_b$ = −200 V). This is attributed to the higher film thickness and the coarsening of the columnar-like structure with overall lower residual stresses which leads to a decrease in hardness [53].

### 3.3. Adhesion behavior of the TiSiN and TiSiCN thin films

The SEM Micrographs of the Rockwell C indents on the TiSiN interlayers and TiSiCN top layers are shown in Fig. 8 with magnifications of the failure areas in secondary electron (SE) and backscattered electron (BSE) mode. The TiSiN interlayer grown at BV of $U_b$ = −100 V exhibits fine networks with cracks and some circular spallations around the indent, which classifies it as HF2. With rising BV, the number of circular cracks and delaminations increases for TiSiN, but the substrate remains unexposed and coated, indicating a cohesive failure. Therefore, the adhesion is categorized as HF3 for $U_b$ = −150 V and HF4 for $U_b$ = −200 V due to the higher number of circular cracks. This can be attributed to the elevated residual stress within the TiSiN interlayer [15].

It is noted that the adhesion behavior of the TiSiN interlayer significantly impacts the adhesion strength of the entire TiSiCN multilayer structure. In this regard, both TiSiCN (1.0 μm) and TiSiCN (2.3 μm) exhibit comparable adhesion behavior depending on the utilized BV for the TiSiN interlayer by decreasing the adhesion strength with increasing BV. For TiSiCN (1.0 μm), an increase in the BV of the TiSiN interlayer results in an increased number of circular cracks. The adhesive failure propagates throughout the complete multilayer structure, partially extending towards the substrate, as represented by the bright areas in the BSE micrographs. In comparison to TiSiCN (1.0 μm), TiSiCN (2.3 μm) shows fewer circular cracks but exhibits enhanced delaminations between the TiSiCN top layer and the TiSiN interlayer. At a higher BV of $U_b$ = −200 V for TiSiN, complete delamination of the entire TiSiCN (2.3 μm) multilayer structure from the substrate occurs. Typically, it has been observed that PVD thin films with greater thicknesses are prone to encountering significant delaminations [54,55]. The dissimilarity in stress distribution and hardness between the TiSiN and TiSiCN layers at the interfaces causes a deterioration in the adhesion behavior [56]. Simultaneously, the stress and hardness properties are influenced by the thickness of the TiSiCN thin film, which further impacts the adhesion behavior. The higher the mismatches between the mechanical properties of the different layers the more likely the adhesion strength decreases.

The critical loads $L_{c2}$ and $L_{c3}$ describe the adhesive failures of the thin film systems and are shown in Fig. 10. At $L_{c2}$ adhesive failure by chipping of the layer at the edge of the scratch track appears. Total failure of the thin film by complete exposure of the substrate occurs at $L_{c3}$. Fig. 9 exemplarily shows SEM micrographs of the entire scratch and the adhesive failures $L_{c2}$ and $L_{c3}$ for TiSiCN (2.3 μm) with TiSiN interlayer deposited at BV of $U_b$ = −100 V. For the TiSiN thin films, a higher BV reduces $L_{c2}$ from (55.7 ± 2.4) N to (29.1 ± 2.9) N. This is attributed to the higher compressive residual stresses within TiSiN, which diminish the adhesion of the thin film to the substrate [4,24]. In contrast, the critical load $L_{c3}$ for TiSiN does not exhibit a clear dependence on the BV, as the $L_{c3}$ values range from (57.4 ± 5.3) N to (60.2 ± 9.3) N without a discernible trend. Therefore, the adhesive failure caused by $L_{c3}$ is neither affected by the stress state nor the hardness of TiSiN.

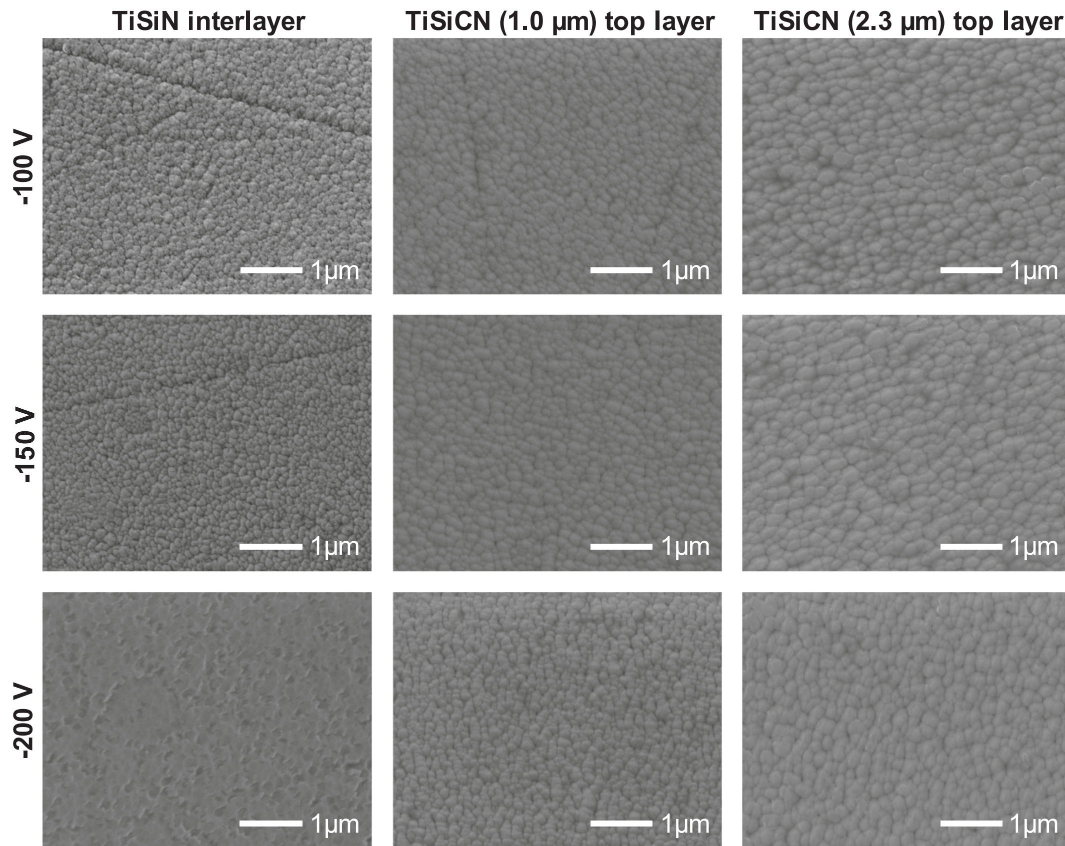


**Fig. 4.** SEM micrographs of the surface morphology of the TiSiN interlayer and the TiSiCN top layer of 1.0 µm and 2.3 µm thickness with TiSiN grown at bias voltages $U_b$ of −100, −150, and − 200 V.

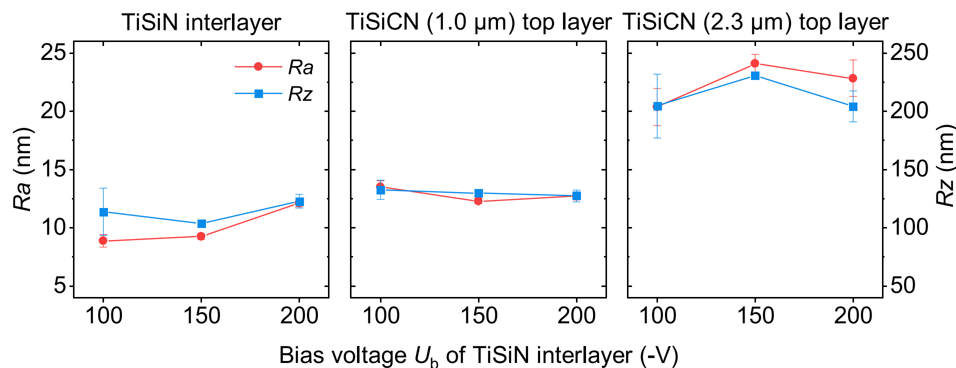


**Fig. 5.** Average mean roughness *Ra* and mean roughness depth *Rz* of the TiSiN interlayer and the TiSiCN top layer of 1.0 µm and 2.3 µm thickness with TiSiN grown at bias voltages $U_b$ of −100, −150, and − 200 V

Among the TiSiCN systems, the highest critical loads were achieved with $L_{c2}$ = (64.4 ± 4.5) N and $L_{c3}$ = (73.4 ± 8.3) N for TiSiCN (1.0 µm) and TiSiCN (2.3 µm) with $L_{c2}$ = (57.4 ± 5.3) N and $L_{c3}$ = (71.6 ± 4.5) N with both having a TiSiN interlayer grown at $U_b$ = −100 V. The increase in the BV of the TiSiN interlayer decreases the adhesion strength of both TiSiCN top layers in terms of $L_{c2}$ and $L_{c3}$. With increasing BV, $L_{c2}$ decreases to (23.2 ± 4.5) N for TiSiCN (1.0 µm) and to (21.4 ± 4.5) N for TiSiCN (2.3 µm). Chipping at $L_{c2}$ is observed between the TiSiCN top layer and the TiSiN interlayer for both thicknesses, as illustrated in Fig. 9, without any apparent exposure of the substrate. Likewise, higher BV for TiSiN results in a reduction of $L_{c3}$ to (50.20 ± 2.2) N for TiSiCN (1.0 µm) and to (58.0 ± 3.6) N for TiSiCN (2.3 µm). The high critical load $L_{c3}$ for the TiSiCN top layers with a TiSiN interlayer deposited at a BV of $U_b$ = −100 V may be attributed to the absorption of the relatively softer TiSiCN top layer, which exhibits lower hardness compared to TiSiN. An increased thickness of the TiSiN interlayer, accompanied by reduced residual stress, contributes to an elevated critical load due to diminished stress transfer [57]. This explains the relatively high critical loads for TiSiCN (2.3 µm) when combined with TiSiN grown at $U_b$ = −150 V, in contrast to TiSiCN (1.0 µm). Furthermore, since the *H*/*E*-ratios for the TiSiCN systems remain nearly constant with the TiSiN interlayers grown at different BV values, the decrease in critical loads $L_{c2}$ and $L_{c3}$ is attributed to the residual stress within the TiSiN interlayers and the differing stress levels between the TiSiN interlayer and TiSiCN top layers. This is particularly evident for $Lc_2$ of the thin film systems with TiSiN deposited at $U_b$ = −200 V, where the difference in hardness and stress between the interfaces of TiSiN and TiSiCN is the highest.

In summary, depositing the TiSiN interlayer at a high BV results in

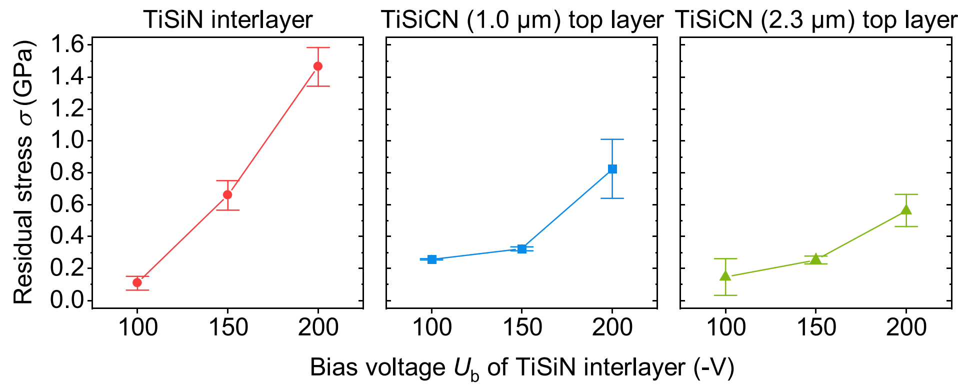


**Fig. 6.** Residual stress of the TiSiN interlayer and the TiSiCN top layer of 1.0 μm and 2.3 μm thickness with TiSiN grown at bias voltages $U_b$ of −100, −150, and − 200 V.

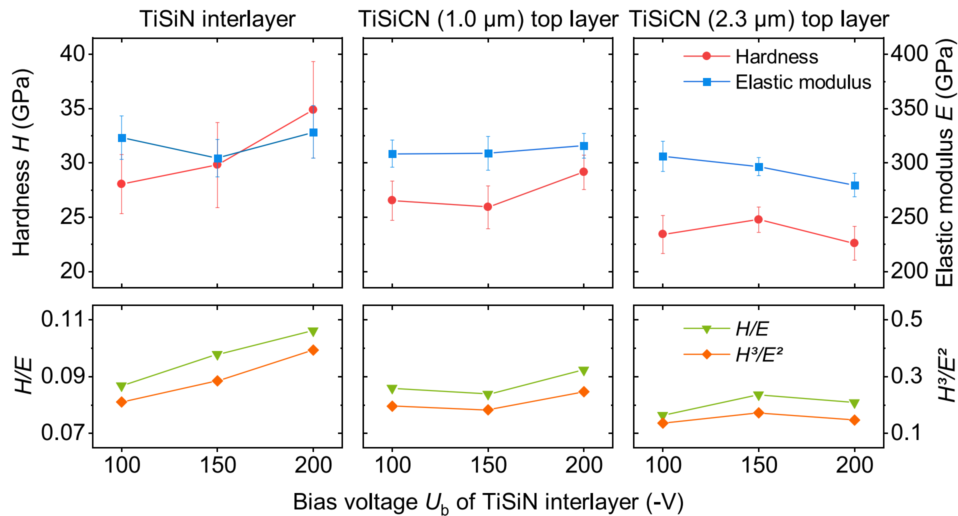


**Fig. 7.** Hardness, elastic modulus, *H/E*, and $H^3/E^2$ of the TiSiN interlayer and the TiSiCN top layer of 1.0 μm and 2.3 μm thickness with TiSiN grown at bias voltages $U_b$ of −100, −150, and − 200 V.

increased residual stresses within TiSiN and leads to a larger stress difference between the TiSiN interlayer and TiSiCN top layers, which promotes adhesion failure. Therefore, reducing this stress difference between the layers within the multilayer structure is necessary to enhance adhesion.

## 4. Conclusion

The BV during the TiSiN synthesis does not only affect the film properties of the TiSiN interlayer it also has a direct impact on the adhesion behavior of the multilayered TiSiCN system. The microstructure of the TiSiN interlayer changes from columnar-like to a denser structure, with the surface morphology transitioning from a cauliflower-like to a crate-like structure and increased roughness due to intensified ion bombardment at higher BV. Furthermore, a higher BV yields higher hardness and compressive stresses within the TiSiN interlayer. The stress state within TiSiN directly influences adhesion behavior, as higher compressive stresses reduce the adhesion strength of the Ti/TiN/TiSiN interlayer system. Higher residual stress within TiSiN deteriorates the adhesion behavior in the form of increased circular cracks in Rockwell C indentation tests and early chipping failure, as reflected by lower $L_{c2}$ values in scratch tests. However, the microstructure and surface morphology of TiSiCN top layers remain unaffected by the changes in structure due to higher ion bombardment of the TiSiN interlayer. The hardness remains relatively unaffected up to a specific degree of structural mismatch between the TiSiN interlayer and the TiSiCN top layer, which can be better compensated by the thicker TiSiCN thin film through its coarser microstructure and is not affected. Nevertheless, the increase in BV of TiSiN interlayer significantly deteriorates the adhesion behavior of the entire Ti/TiN/TiSIN/TiSiCN multilayer structure. Increased residual stresses within the TiSiN interlayer reduce the adhesion strength of the TiSiCN multilayer structure. Furthermore, increasing the thickness of the TiSiCN top layer decreases the adhesion strength of the entire thin film system. The TiSiN interlayer deposited at a BV of $U_b$ = −100 V, favors a multilayered TiSiCN structure with enhanced adhesion strength. Here, the stress and hardness differences are minimized, enabling the softer TiSiCN thin film to absorb the stresses resulting from substrate/thin film system deformation in the Rockwell C test and scratch test. Additionally, the higher thickness of TiSiCN (2.3 μm), featuring a coarser structure and lower hardness, reduced the residual stress of the entire multilayer system.

Overall, the Ti/TiN/TiSiN is suitable as an interlayer system, which can be adapted by choosing a suitable bias voltage to the mechanical and structural properties of the TiSiCN top layer. The results highlight that a smaller difference in hardness and residual stress between the TiSiN interlayer and TiSiCN top layer is favorable for better adhesion behavior of the thin film system.

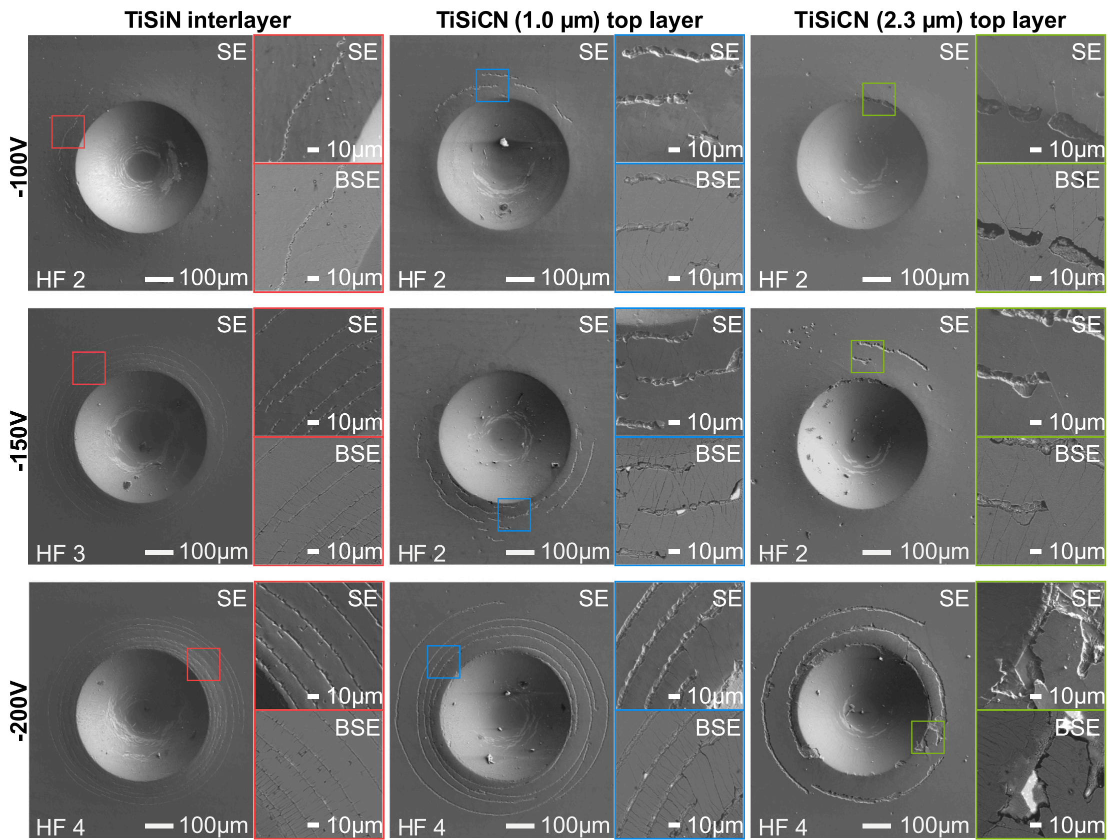


**Fig. 8.** SEM micrographs of the Rockwell indents of the TiSiN interlayer and the TiSiCN top layer of 1.0 µm and 2.3 µm thickness with TiSiN grown at bias voltages $U_b$ of −100, −150, and − 200 V.

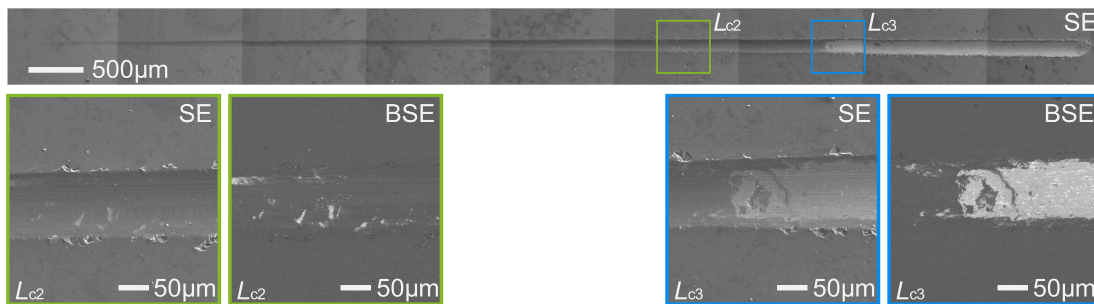


**Fig. 9.** SEM micrographs of $L_{c2}$ and $L_{c3}$ on an exemplary scratch of TiSiCN (2.3 µm) with TiSiN interlayer deposited at BV of $U_b$ = −100 V.

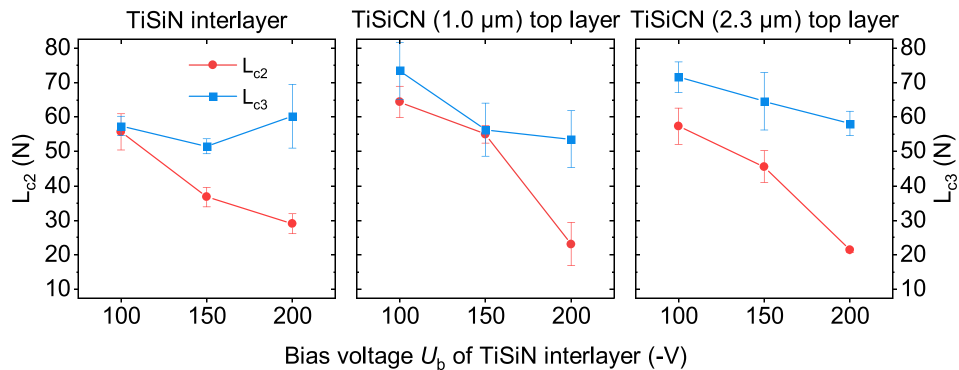


**Fig. 10.** Critical loads $L_{c2}$ and $L_{c3}$ of the TiSiN interlayer and the TiSiCN top layer of 1.0 µm and 2.3 µm thickness with TiSiN grown at bias voltages $U_b$ of −100, −150, and − 200 V.

## CRediT authorship contribution statement

**Wolfgang Tillmann:** Resources, Supervision, Writing – review & editing. **Julia Urbanczyk:** Conceptualization, Investigation, Project administration, Visualization, Writing – original draft. **Alexander Thewes:** Writing – review & editing. **Günter Bräuer:** Writing – review & editing. **Nelson Filipe Lopes Dias:** Supervision, Writing – review & editing.

## Declaration of generative AI and AI-assisted technologies in the writing process

During the preparation of this work, the authors used ChatGPT and DeepL to improve language and readability. After using these tools, the authors reviewed and edited the content as needed and take full responsibility for the content of the publication.

## Declaration of competing interest

The authors declare that they have no known competing financial interests or personal relationships that could have appeared to influence the work reported in this paper.

## Data availability

Data will be made available on request.

## Acknowledgments

This work was supported by the German Research Foundation (DFG) within the project 434108570 (grant numbers TI 343/180-1 and BR 2178-59-1). The authors gratefully acknowledge the Institute of Machining Technology (ISF), Dortmund for providing confocal microscopy.

## References

[1] T. Polcar, T. Kubart, R. Novák, L. Kopecký, P. Široký, Comparison of tribological behaviour of TiN, TiCN and CrN at elevated temperatures, Surf. Coat. Technol. 193 (2005) 192–199, https://doi.org/10.1016/j.surfcoat.2004.07.098.
[2] N. Madaoui, N. Saoula, B. Zaid, D. Saidi, A.S. Ahmed, Structural, mechanical and electrochemical comparison of TiN and TiCN coatings on XC48 steel substrates in NaCl 3.5% water solution, Appl. Surf. Sci. 312 (2014) 134–138, https://doi.org/10.1016/j.apsusc.2014.04.167.
[3] Y.Y. Guu, J.F. Lin, C.-F. Ai, The tribological characteristics of titanium nitride, titanium carbonitride and titanium carbide coatings, Thin Solid Films 302 (1997) 193–200, https://doi.org/10.1016/S0040-6090(96)09546-6.
[4] R. Akhter, Z. Zhou, Z. Xie, P. Munroe, TiN versus TiSiN coatings in indentation, scratch and wear setting, Appl. Surf. Sci. 563 (2021) 150356, https://doi.org/10.1016/j.apsusc.2021.150356.
[5] N. Jiang, Y. Shen, Y.-W. Mai, T. Chan, S.C. Tung, Nanocomposite Ti–Si–N films deposited by reactive unbalanced magnetron sputtering at room temperature, Mater. Sci. Eng. B 106 (2004) 163–171, https://doi.org/10.1016/j.mseb.2003.09.033.
[6] M. Diserens, J. Patscheider, F. Lévy, Improving the properties of titanium nitride by incorporation of silicon, Surf. Coat. Technol. 108-109 (1998) 241–246, https://doi.org/10.1016/S0257-8972(98)00560-X.
[7] J.-H. Jeon, S.R. Choi, W.S. Chung, K.H. Kim, Synthesis and characterization of quaternary Ti–Si–C–N coatings prepared by a hybrid deposition technique, Surf. Coat. Technol. 188-189 (2004) 415–419, https://doi.org/10.1016/j.surfcoat.2004.08.042.
[8] W. Li, P. Liu, Z. Xue, F. Ma, K. Zhang, X. Chen, R. Feng, P.K. Liaw, Microstructures, mechanical behavior and strengthening mechanism of TiSiCN nanocomposite films, Sci. Rep. 7 (2017) 2140, https://doi.org/10.1038/s41598-017-02186-1.
[9] A.A. Onoprienko, V.I. Ivashchenko, S.N. Dub, O. Khyzhun, I.I. Timofeeva, Microstructure and mechanical properties of hard Ti–Si–C–N films deposited by dc magnetron sputtering of multicomponent Ti/C/Si target, Surf. Coat. Technol. 205 (2011) 5068–5072, https://doi.org/10.1016/j.surfcoat.2011.05.009.
[10] I. Endler, M. Höhn, J. Schmidt, S. Scholz, M. Herrmann, M. Knaut, Ternary and quarternary TiSiN and TiSiCN nanocomposite coatings obtained by chemical vapor deposition, Surf. Coat. Technol. 215 (2013) 133–140, https://doi.org/10.1016/j.surfcoat.2012.10.067.
[11] K.A. Kuptsov, P. Kiryukhantsev-Korneev, A.N. Sheveyko, D.V. Shtansky, Comparative study of electrochemical and impact wear behavior of TiCN, TiSiCN, TiCrSiCN, and TiAlSiCN coatings, Surf. Coat. Technol. 216 (2013) 273–281. doi:10.1016/j.surfcoat.2012.11.058.
[12] H. Xu, X. Nie, R. Wei, Tribological behavior of a TiSiCN coating tested in air and coolant, Surf. Coat. Technol. 201 (2006) 4236–4241, https://doi.org/10.1016/j.surfcoat.2006.08.066.
[13] S. Abraham, E.Y. Choi, N. Kang, K.H. Kim, Microstructure and mechanical properties of Ti-Si-C-N films synthesized by plasma-enhanced chemical vapor deposition, Surf. Coat. Technol. 202 (2007) 915–919, https://doi.org/10.1016/j.surfcoat.2007.05.073.
[14] S. Imamura, H. Fukui, A. Shibata, N. Omori, M. Setoyama, Properties and cutting performance of AlTiCrN/TiSiCN bilayer coatings deposited by cathodic-arc ion plating, Surf. Coat. Technol. 202 (2007) 820–825, https://doi.org/10.1016/j.surfcoat.2007.05.087.
[15] C.-L. Chang, T.-J. Hsieh, Effect of C2H2 gas flow rate on synthesis and characteristics of Ti–Si–C–N coating by cathodic arc plasma evaporation, J. Mater. Process. Technol. 209 (2009) 5521–5526, https://doi.org/10.1016/j.jmatprotec.2009.05.008.
[16] M. Azadi, A. Sabour Rouhaghdam, S. Ahangarani, Properties of TiC coating by pulsed DC PACVD, Journal of Coatings 2013 (2013) 1–6. doi:101155/2013/712812.
[17] M. Abedi, A. Abdollah-zadeh, A. Vicenzo, M. Bestetti, F. Movassagh-Alanagh, E. Damerchi, A comparative study of the mechanical and tribological properties of PECVD single layer and compositionally graded TiSiCN coatings, Ceram. Int. 45 (2019) 21200–21207, https://doi.org/10.1016/j.ceramint.2019.07.100.
[18] W. Tillmann, N.F. Lopes Dias, C. Franke, D. Kokalj, D. Stangier, C.A. Thomann, J. Debus, Mechanical properties and adhesion behavior of amorphous carbon films with bias voltage controlled TixCy interlayers on Ti6Al4V, Diam. Relat. Mater. 115 (2021) 108361, https://doi.org/10.1016/j.diamond.2021.108361.
[19] Y. Wang, J. Li, C. Dang, Y. Wang, Y. Zhu, Influence of carbon contents on the structure and tribocorrosion properties of TiSiCN coatings on Ti6Al4V, Tribol. Int. 109 (2017) 285–296, https://doi.org/10.1016/j.triboint.2017.01.002.
[20] K. Chu, P.W. Shum, Y.G. Shen, Substrate bias effects on mechanical and tribological properties of substitutional solid solution (Ti, Al)N films prepared by reactive magnetron sputtering, Mater. Sci. Eng. B 131 (2006) 62–71, https://doi.org/10.1016/j.mseb.2006.03.036.
[21] C.-L. Chang, C.-T. Lin, P.-C. Tsai, W.-Y. Ho, D.-Y. Wang, Influence of bias voltages on the structure and wear properties of TiSiN coating synthesized by cathodic arc plasma evaporation, Thin Solid Films 516 (2008) 5324–5329, https://doi.org/10.1016/j.tsf.2007.07.087.
[22] Y. Zhang, Y. Yang, Y. Zhai, P. Zhang, Effect of negative substrate bias on the microstructure and mechanical properties of Ti–Si–N films deposited by a hybrid filtered cathodic arc and ion beam sputtering technique, Appl. Surf. Sci. 258 (2012) 6897–6901, https://doi.org/10.1016/j.apsusc.2012.03.127.
[23] C.T. Guo, D. Lee, P.C. Chen, Deposition of TiSiN coatings by arc ion plating process, Appl. Surf. Sci. 254 (2008) 3130–3136, https://doi.org/10.1016/j.apsusc.2007.10.079.
[24] R. Akhter, Z. Zhou, Z. Xie, P. Munroe, Influence of substrate bias on the scratch, wear and indentation response of TiSiN nanocomposite coatings, Surf. Coat. Technol. 425 (2021) 127687. doi:10.1016/j.surfcoat.2021.127687.
[25] G. Janssen, M.M. Abdalla, F. van Keulen, B.R. Pujada, B. van Venrooy, Celebrating the 100th anniversary of the Stoney equation for film stress: developments from polycrystalline steel strips to single crystal silicon wafers, Thin Solid Films 517 (2009) 1858–1867, https://doi.org/10.1016/j.tsf.2008.07.014.
[26] W.C. Oliver, G.M. Pharr, An improved technique for determining hardness and elastic modulus using load and displacement sensing indentation experiments, J. Mater. Res. 7 (1992) 1564–1583, https://doi.org/10.1557/JMR.1992.1564.
[27] S. Peng, J. Xu, P. Munroe, Z. Xie, Sandwich-structured, damage-resistant TiN/graded TiSiN/TiSiN film, Results in Physics 12 (2019) 543–554, https://doi.org/10.1016/j.rinp.2018.12. 019.
[28] X. Zhao, Z. Xie, P. Munroe, Nanoindentation of hard multilayer coatings: finite element modelling, Mater. Sci. Eng. A 528 (2011) 1111–1116, https://doi.org/10.1016/j.msea.2010.09.073.
[29] DIN 4856:2018–02, Kohlenstoffschichten und andere Hartstoffschichten_-Rockwell-Eindringprüfung zur Bewertung der Haftung, Beuth Verlag GmbH, Berlin.
[30] DIN EN ISO 20502:2016–11, Hochleistungskeramik_- Bestimmung der Haftung von keramischen Schichten mit dem Ritztest (ISO_20502:2005 einschließlich Cor_1: 2009); Deutsche Fassung EN_ISO_20502:2016, Beuth Verlag GmbH, Berlin.
[31] J. Vlček, M. Kormunda, J. Čízek, V. Peřina, J. Zemek, Influence of nitrogen–argon gas mixtures on reactive magnetron sputtering of hard Si–C–N films, Surf. Coat. Technol. 160 (2002) 74–81, https://doi.org/10.1016/S0257-8972(02)00328-6.
[32] J.H. Kim, K.W. Chung, Microstructure and properties of silicon nitride thin films deposited by reactive bias magnetron sputtering, J. Appl. Phys. 83 (1998) 5831–5839, https://doi.org/10.1063/1.367440.
[33] J. Houška, J. Vlček, Š. Potocký, V. Peřina, Influence of substrate bias voltage on structure and properties of hard Si–B–C–N films prepared by reactive magnetron sputtering, Diam. Relat. Mater. 16 (2007) 29–36, https://doi.org/10.1016/j.diamond. 2006.03.012.
[34] D.M. Devia, E. Restrepo-Parra, P.J. Arango, A.P. Tschiptschin, J.M. Velez, TiAlN coatings deposited by triode magnetron sputtering varying the bias voltage, Appl. Surf. Sci. 257 (2011) 6181–6185, https://doi.org/10.1016/j.apsusc.2011.02.027.
[35] M. Arab Pour Yazdi, F. Lomello, J. Wang, F. Sanchette, Z. Dong, T. White, Y. Wouters, F. Schuster, A. Billard, Properties of TiSiN coatings deposited by hybrid HiPIMS and pulsed-DC magnetron co-sputtering, Vacuum 109 (2014) 43–51, https://doi.org/10.1016/j.vacuum.2014.06.023.

[36] J. Patscheider, T. Zehnder, M. Diserens, Structure–performance relations in nanocomposite coatings, Surf. Coat. Technol. 146-147 (2001) 201–208, https://doi.org/10.1016/S0257-8972(01)01389-5.

[37] T.Q. Li, S. Noda, Y. Tsuji, T. Ohsawa, H. Komiyama, Initial growth and texture formation during reactive magnetron sputtering of TiN on Si(111), J. Vac. Sci. Technol. A 20 (2002) 583–588, https://doi.org/10.1116/1.1458944.

[38] R. Shuangquan, H. Jun, W. Hongjun, T. Canxin, G. Liping, F. Dejun, Effects of Bias voltage on the structure and mechanical properties of thick CrN coatings deposited by mid-frequency magnetron sputtering, Plasma Sci. Technol. 11 (2009) 38–41, https://doi.org/10.1088/1009-0630/11/1/08.

[39] Y. Wang, J. Li, C. Dang, Y. Wang, Y. Zhu, Influence of bias voltage on structure and tribocorrosion properties of TiSiCN coating in artificial seawater, Mater. Charact. 127 (2017) 198–208, https://doi.org/10.1016/j.matchar.2017.03.012.

[40] J. Lin, R. Wei, A comparative study of thick TiSiCN nanocomposite coatings deposited by dcMS and HiPIMS with and without PEMS assistance, Surf. Coat. Technol. 338 (2018) 84–95, https://doi.org/10.1016/j.surfcoat.2018.01.082.

[41] Z.T. Yang, B. Yang, L.P. Guo, D.J. Fu, Effect of bias voltage on the structure and hardness of TiSiN composite coatings synthesized by cathodic arc assisted middle-frequency magnetron sputtering, J. Alloys Compd. 473 (2009) 437–441, https://doi.org/10.1016/j.jallcom.2008.06.003.

[42] I. Petrov, P.B. Barna, L. Hultman, J.E. Greene, Microstructural evolution during film growth, J. Vac. Sci. Technol. A 21 (2003) S117–S128, https://doi.org/10.1116/1.1601610.

[43] H. Oettel, R. Wiedemann, S. Preißler, Residual stresses in nitride hard coatings prepared by magnetron sputtering and arc evaporation, Surf. Coat. Technol. 74-75 (1995) 273–278, https://doi.org/10.1016/0257-8972(95)08235-2.

[44] A. Moridi, H. Ruan, L.C. Zhang, M. Liu, Residual stresses in thin film systems: effects of lattice mismatch, thermal mismatch and interface dislocations, Int. J. Solids Struct. 50 (2013) 3562–3569, https://doi.org/10.1016/j.ijsolstr.2013.06.022.

[45] K. Fischer, H. Oettel, Microstructural gradients in thin hard coatings—tailor-made, Surf. Coat. Technol. 97 (1997) 308–312, https://doi.org/10.1016/S0257-8972(97)00377-0.

[46] J.-H. Huang, C.-H. Ma, H. Chen, Effect of Ti interlayer on the residual stress and texture development of TiN thin films, Surf. Coat. Technol. 200 (2006) 5937–5945, https://doi.org/10.1016/j.surfcoat.2005.09.005.

[47] F. Li, S. Zhang, J. Kong, Y. Zhang, W. Zhang, Multilayer DLC coatings via alternating bias during magnetron sputtering, Thin Solid Films 519 (2011) 4910–4916, https://doi.org/10.1016/j.tsf.2011.01.052.

[48] M. Nose, Y. Deguchi, T. Mae, E. Honbo, T. Nagae, K. Nogi, Influence of sputtering conditions on the structure and properties of Ti–Si–N thin films prepared by r.f.-reactive sputtering, Surf. Coat. Technol. 174-175 (2003) 261–265, https://doi.org/10.1016/S0257-8972(03)00710-2.

[49] S. Veprek, M.G. Veprek-Heijman, P. Karvankova, J. Prochazka, Different approaches to superhard coatings and nanocomposites, Thin Solid Films 476 (2005) 1–29. doi:10.1016/j.tsf.2004.10.053.

[50] J. Musil, Hard and superhard nanocomposite coatings, Surf. Coat. Technol. 125 (2000) 322–330, https://doi.org/10.1016/S0257-8972(99)00586-1.

[51] H.-M. Lin, J.-G. Duh, R. Wei, C. Rincon, J.-W. Lee, The effect of microstructure and composition on mechanical properties in thick-layered nanocomposite Ti–Si–C–N coatings, Surf. Coat. Technol. 205 (2010) 1460–1464, https://doi.org/10.1016/j.surfcoat.2010.07.070.

[52] S.L. Ma, D.Y. Ma, Y. Guo, B. Xu, G.Z. Wu, K.W. Xu, P.K. Chu, Synthesis and characterization of super hard, self-lubricating Ti–Si–C–N nanocomposite coatings, Acta Mater. 55 (2007) 6350–6355, https://doi.org/10.1016/j.actamat.2007.07.046.

[53] N.G. Demas, C. Lorenzo-Martin, O.O. Ajayi, R.A. Erck, I. Shareef, Measurement of thin-film coating hardness in the presence of contamination and roughness: implications for tribology, Metall. Mat. Trans. A 47 (2016) 1629–1640, https://doi.org/10.1007/s11661-016-3342-9.

[54] W. Heinke, A. Leyland, A. Matthews, G. Berg, C. Friedrich, E. Broszeit, Evaluation of PVD nitride coatings, using impact, scratch and Rockwell-C adhesion tests, Thin Solid Films 270 (1995) 431–438, https://doi.org/10.1016/0040-6090(95)06934-8.

[55] P.J. Burnett, D.S. Rickerby, The scratch adhesion test: an elastic-plastic indentation analysis, Thin Solid Films 157 (1988) 233–254, https://doi.org/10.1016/0040-6090(88)90006-5.

[56] S. PalDey, S. Deevi, Single layer and multilayer wear resistant coatings of (Ti,Al)N: a review, Mater. Sci. Eng. A 342 (2003) 58–79, https://doi.org/10.1016/S0921-5093(02)00259-9.

[57] K. Wasa, M. Kitabatake, H. Adachi, Thin Film Materials Technology: Sputtering of Compound Materials, William Andrew Pub, Norwich, NY, 2004.